Fast ion absorption of the high harmonic fast wave in the National Spherical Torus Experiment[a)]

A. L. Rosenberg,[b)] J. E. Menard, J. R. Wilson, S. S. Medley, R. Andre, C. K. Phillips, D. S. Darrow, B. P. LeBlanc, M. H. Redi, N. J. Fisch, and the NSTX Team
Princeton Plasma Physics Laboratory, Princeton, New Jersey 08543

R. W. Harvey
CompX, Del Mar, California 92014

T. K. Mau
University of California at San Diego, La Jolla, California 92093

E. F. Jaeger, P. M. Ryan, and D. W. Swain
Oak Ridge National Laboratory, Oak Ridge, Tennessee 37831

S. A. Sabbagh
Department of Applied Physics and Applied Mathematics, Columbia University, New York, New York 10027

J. Egedal
Plasma Science and Fusion Center, Massachusetts Institute of Technology, Cambridge, Massachusetts 02139

(Received 23 October 2003; accepted 19 December 2003; published online 23 April 2004)

Ion absorption of the high harmonic fast wave in a spherical torus [Y.-K. M. Peng *et al.*, Nucl. Fusion **26**, 769 (1986)] is of critical importance to assessing the viability of the wave as a means of heating and driving current. Analysis of recent National Spherical Torus Experiment [M. Ono *et al.*, Nucl. Fusion **40**, 557 (2000)] shots has revealed that under some conditions when neutral beam and rf power are injected into the plasma simultaneously, a fast ion population with energy above the beam injection energy is sustained by the wave. In agreement with modeling, these experiments find the rf-induced fast ion tail strength and neutron rate at lower *B*-fields to be less enhanced, likely due to a larger β profile, which promotes greater off-axis absorption where the fast ion population is small. Ion loss codes find the increased loss fraction with decreased *B* insufficient to account for the changes in tail strength, providing further evidence that this is a rf interaction effect. Though greater ion absorption is predicted with lower $k_{\|}$, surprisingly little variation in the tail was observed, along with a neutron rate enhancement with higher $k_{\|}$. Data from the neutral particle analyzer, neutron detectors, x-ray crystal spectrometer, and Thomson scattering are presented, along with results from the TRANSP [R. J. Hawryluk, Physics of Plasmas Close to Thermonuclear Conditions **1**, 19 (1981); J. P. H. E. Ongena *et al.*, Fusion Technol. **33**, 181 (1998)] transport analysis code, ray-tracing codes HPRT [J. Menard *et al.*, Phys. Plasmas **6**, 2002 (1999)], and CURRAY [T. K. Mau *et al.*, RF Power in Plasmas: 13th Topical Conference (1999), p. 148], full-wave code AORSA [E. F. Jaeger *et al.*, RF Power in Plasmas: 14th Topical Conference, 2001, p. 369], quasilinear code CQL3D [R. W. Harvey *et al.*, in Proceedings of the IAEA TCM on Advances in Simulation and Modeling of Thermonuclear Plasmas, 1992], and ion loss codes EIGOL [D. S. Darrow *et al.*, in Proceedings of the 6th IAEA TCM on Energetic Particles in Magnetic Confinement Systems, 2000, p. 109] and CONBEAM [J. Egedal *et al.*, Phys. Plasmas **10**, 2372 (2003)]. © *2004 American Institute of Physics.*
[DOI: 10.1063/1.1651099]

I. INTRODUCTION AND MOTIVATION

Interaction between the high harmonic fast wave (HHFW) and energetic particles in a spherical torus (ST) (Ref. 1) is a new and important research area. A fast ion population of fusion-born alpha particles will be found in a reacting plasma, along with energetic ions from neutral beam injection (NBI) in some scenarios. First investigated in Ref. 2, HHFW is currently being explored as a means of heating and driving plasma current in such plasmas, which have a significantly larger β, steeper profile gradients, and more closely spaced harmonic layers than conventional aspect ratio tokamaks. In the National Spherical Torus Experiment's (NSTX's) (Ref. 3) most recent campaigns, a clear fast ion tail was observed on the neutral particle analyzer (NPA),[4] when HHFW and NBI were active simultaneously. Increases in neutron detector signals provided further evidence for interaction between neutral beam ions and the wave. This was observed for nearly every shot in which a significant overlap in rf and NBI power was present. A ray-tracing code was used to analyze these shots, and absorption by fast ions was predicted to be competitive with electron absorption. Mea-

[a)]Paper GI2 4, Bull. Am. Phys. Soc. **48**, 126 (2003).
[b)]Invited speaker. Electronic mail: arosenbe@pppl.gov

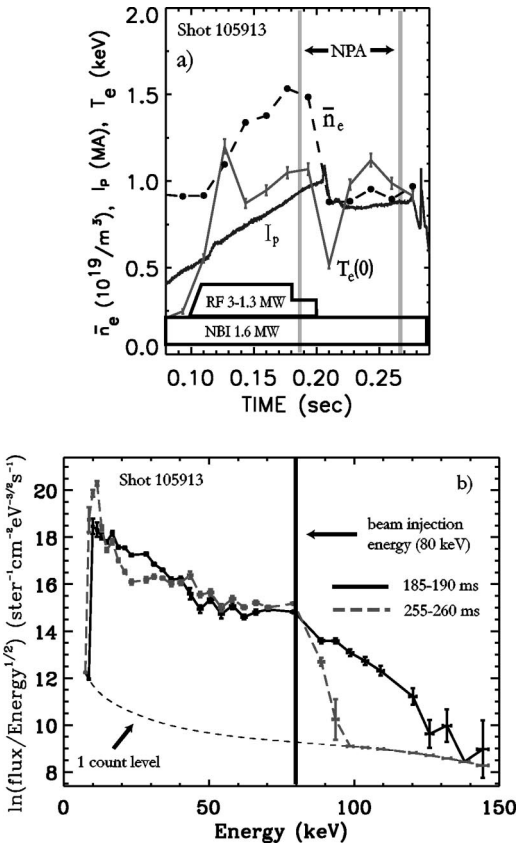

FIG. 1. (a) Line-averaged density, temperature, plasma current, NBI, and rf power histories for NSTX shot 105913. Note the rf power drops from 3 MW to 1.3 MW at 180 ms. (b) Neutral particle analyzer spectra for 2 time windows, the first during rf, the second after.

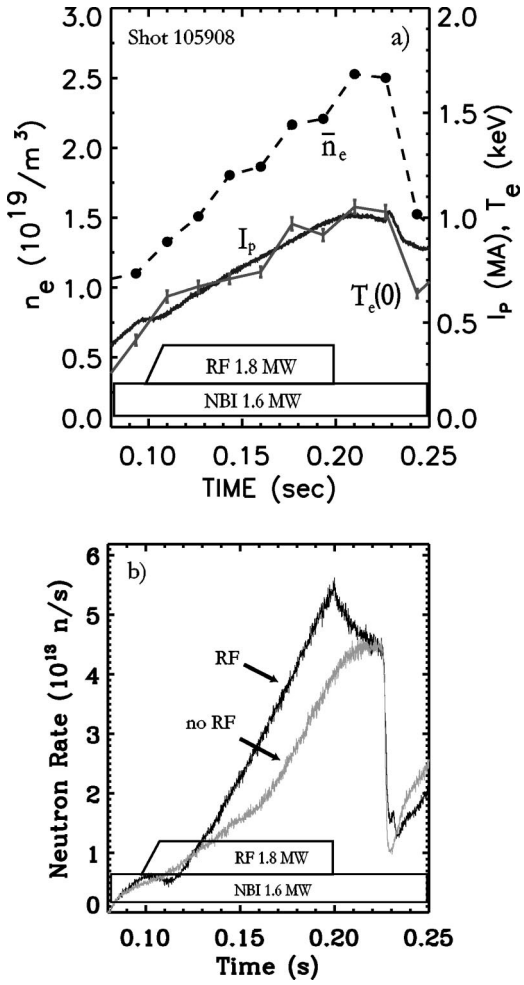

FIG. 2. (a) Typical parameters for neutron rate comparison. (b) Neutron rates for NSTX shots 105906 (no rf) and 105908 (rf). A significant rf-induced enhancement in the neutron rate is observed before the MHD event, which occurred in both shots at $t=226$ ms.

sured neutron rates for similar rf and no-rf shots were compared with predicted rates, and a significant rf-induced enhancement was found, consistent with the enhanced tail. The rf frequency of the antenna in NSTX is 30 MHz, and typical deuterium harmonic numbers range from 9 on-axis to 13 near the edge of the plasma. Evidence for rf-induced current drive without NBI in NSTX is presented in Ref. 5.

II. EXPERIMENTAL STUDIES

A. Beam heated shots with and without rf

Two separate run days on NSTX were devoted to examining the effect of HHFW on a neutral beam heated plasma. One was the shot set 1059XX, where rf and NBI were injected early in the discharge in an attempt to affect the plasma current evolution. Plasma parameters and NPA spectra before and after rf turnoff for shot 105913 are shown in Fig. 1. For all shots analyzed, the neutral beam injected deuterium neutrals into the plasma with an energy $E_{\mathrm{beam}} \approx 80\,\mathrm{keV}$ and a total power $P_{\mathrm{beam}} \approx 1.6\,\mathrm{MW}$. Without rf, the energy spectrum observed by the NPA decreased rapidly above ~80 keV. With rf, the energy spectrum extended to ~130 keV. Unfortunately, there was no shot in this set when the NPA and neutron detectors were functioning properly simultaneously. Also, a large MHD event upon rf turnoff in shots with the NPA operating prevented a proper examination of the fast ion tail decay. Nevertheless, the effect of rf on this plasma was able to be observed.

The ZnS neutron detector saw a significant signal enhancement with rf. This signal, which is heavily weighted to the high energy end of the fast ion spectrum, declined immediately upon rf turnoff. As shown in Fig. 2, for similar shots with and without rf, within 25 ms of rf turnoff the enhanced neutron rate decayed to the no-rf value.

Several months later, a full run day was dedicated to further investigating interaction between HHFW and fast ions. Here, shot series 1082XX, rf was injected at 200 ms, 20 ms after the plasma current had reached its flat top. In spite of a MHD event at 240 ms for nearly every shot in this series, several clear trends were still observed. Typical parameters for this set of shots are shown in Fig. 3(a). After rf turnoff with NBI remaining active, the tail decayed to the no-rf spectrum on a time scale comparable to that for decay of a beam-only distribution after NBI turnoff, as seen in Fig. 3(b). Neutron rates and NPA spectra for similar rf vs no-rf shots in identical time ranges are shown in Fig. 4.

Holding other parameters fixed, a horizontal NPA scan

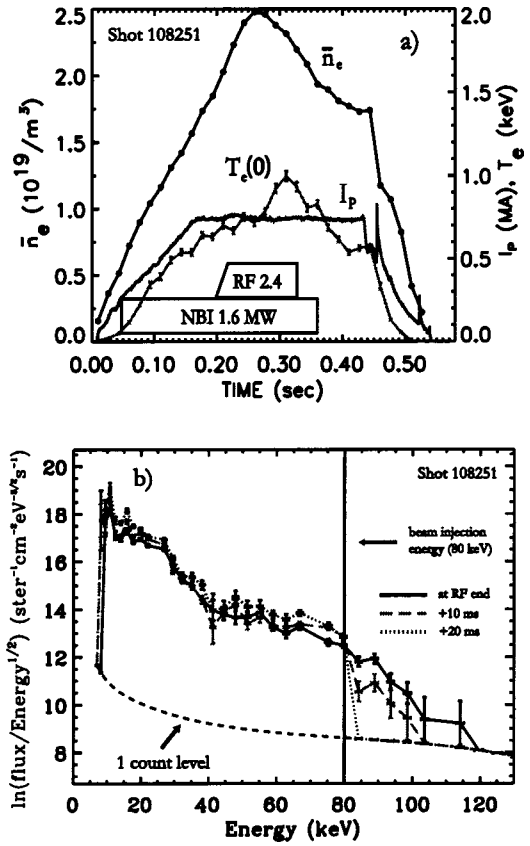

FIG. 3. (a) Typical line-averaged density, temperature, plasma current, NBI, and rf power histories for scans in recent experiments. (b) Neutral particle analyzer data for NSTX shot 108251, $B_0=4.5$ kG, launched $k_\parallel=14\ \mathrm{m}^{-1}$ (heating phasing), after rf turns off at $t=320$ ms. The signal labeled ''at rf end'' is averaged from 310 to 320 ms, the ''+10 ms'' curve is averaged from 320 to 330 ms, and the ''+20 ms'' curve is averaged from 335 to 340 ms. The fast ion population above 80 keV beam injection energy collapses to a typical no-rf distribution within 20 ms.

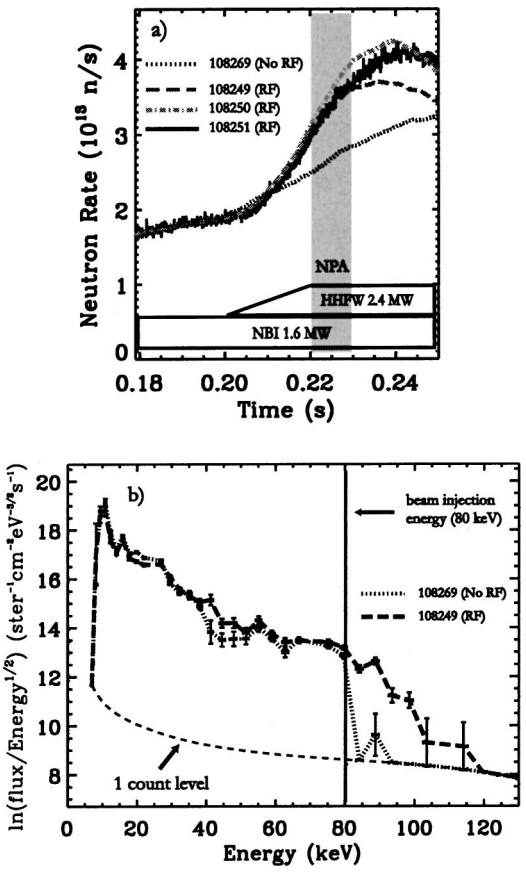

FIG. 4. (a) Neutron rates for shots with and without rf. The NPA was horizontally scanned for shots 108249–108251, but otherwise no changes in shot setup were made. $B_0=4.5$ kG, $\beta_t\approx5.2\%$, $k_\parallel=14\ \mathrm{m}^{-1}$. (b) NPA spectra at a sightline tangency radius of 70 cm for NSTX shots 108249 (rf) and 108269 (no-rf), averaged from 220 to 230 ms. A clear rf-induced fast ion population above the beam injection energy is observed.

was performed for most shots in this series, aside from the no-rf shot 108269. Although shot 108249 is the only $k_\parallel=14\ \mathrm{m}^{-1}$ shot with the NPA at the same tangency radius and basic plasma parameters as the no-rf shot, the neutron rate compared with the two others in the NPA scan indicates this may not be the ideal shot to analyze. As such, more concentration is placed on shots 108250 and 108251 in subsequent studies. 108251 is particularly interesting as its sightline tangency radius is 90 cm, and crosses the beam path within a few centimeters of the magnetic axis. The NPA scan is shown in Fig. 5.

The similarity between signals at 70 cm and 90 cm may be understood by noting the competing effects of pitch angle and neutral particle density localization. At 70 cm, within 1 cm of the beam injection tangency radius of 69.4 cm, a particle would have to pitch angle scatter far less to find its way to the neutral particle analyzer. However, the beam and background neutral density is lower at this location. At 90 cm, the beam density is much greater, though a particle would have to pitch angle scatter more to arrive at the NPA. At 50 cm, the neutral and fast ion density are lower, so the lower signal is understandable. An outboard ($R_{\tan}>R_{\mathrm{axis}}$) NPA scan should show a cleaner trend, however, this scan was not possible during this run period.

B. Magnetic field scan

To further examine the fast ion absorption dependence on various parameters, scans in B_0 and $k_\parallel$ were performed. In

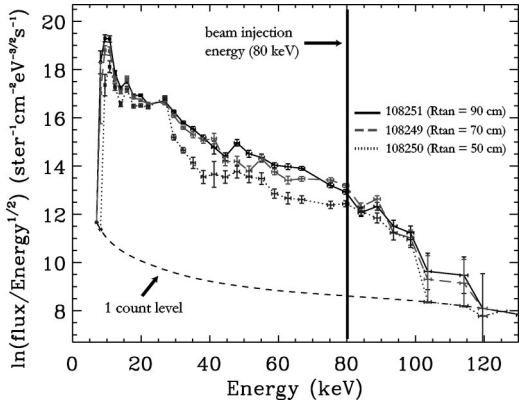

FIG. 5. Horizontal NPA scan for otherwise identical shots, averaged from 220 to 230 ms. $B_0=4.5$ kG, $\beta_t\approx5.2\%$, $k_\parallel=14\ \mathrm{m}^{-1}$. The magnetic axis is at ≈100 cm for these shots. The beam tangency radius is at 69.4 cm, and the 90 cm sightline crosses the beam within 4 cm of the magnetic axis.

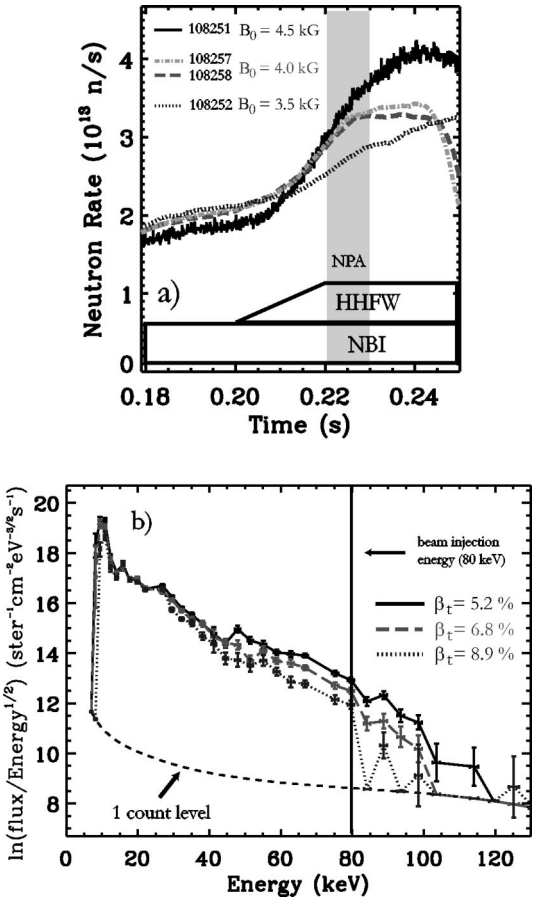

FIG. 6. (a) Neutron rates for otherwise similar NSTX shots at $B_0=3.5$, 4.0, and 4.5 kG, which correspond to $\beta_t \approx 5.2\%$, 6.8%, and 8.9%, respectively. (b) NPA signals at $R_{\tan}=90$ cm for B_0 scan, averaged over time window displayed in (a). The larger β profile at lower B_0 may promote greater off-axis electron absorption, reducing the fraction of power available to the centralized fast ion population.

Ref. 2, off-axis electron absorption is predicted to increase with β. As changes in kinetic profiles between shots were relatively small compared to changes in B^2, the magnetic field scan effectively became a β scan as well. As demonstrated in Fig. 6, the neutron rate was found to decrease with decreasing toroidal field, and the fast ion tail on the NPA dropped to nearly a no-rf spectrum. A plausible explanation is that the larger β profile at lower B_0 promotes greater off-axis electron absorption, reducing the fraction of power available to the centralized fast ion population.

Traces of $T_e(0)$, $\overline{n_e}$, I_p, rf power, and beam power for the high and low B_0 shots in the scan are shown in Figs. 7(a) and 7(b). The large difference in $\beta_{te}=n_eT_e/B_t^2$ profiles on the outer midplane is demonstrated in Fig. 7(c). These shots have very similar electron temperature profiles, as shown in Fig. 7(d), however, the electron density is found to be somewhat larger in the low B_0, high β shot, as shown in Fig. 7(e). Line-averaged Z_{eff} is also measured to be lower (2.35 vs 2.79) in the low B_0 shot, leading to a significantly larger thermal deuterium profile, shown in Fig. 7(f), if one assumes a flat Z_{eff} profile. The fast ion density profiles as computed by transport analysis code TRANSP (Refs. 6 and 7) are also shown in Fig. 7(g). As neutron rate is roughly proportional to thermal deuterium density times fast ion density—a profile of this product, n_dn_f, is shown in Fig. 7(h)—one would expect a larger neutron rate at the higher β shot, which is, in fact, what is observed before the rf turns on in Fig. 6(a). The rf then proceeds to pump the low β, high B rate to well above the high β, low B rate. A plot of neutron rates normalized to n_dn_f is shown in Fig. 7(i). Comparing Figs. 7(i) and 6(a), the observed neutron rate difference may have been even larger if the densities were equal.

C. $k_\parallel$ scan

Though greater ion absorption is predicted with lower $k_\parallel$,[8,9] a somewhat larger neutron rate enhancement and rf-induced tail was observed with higher $k_\parallel$. Results are shown in Fig. 8. Kinetic histories for these shots are quite similar, as shown in Fig. 9. Although a stronger heating result with countercurrent drive phasing has been observed in recent current drive experiments without neutral beam heating on NSTX,[5] varying directionality of the $k_\parallel=7\ \text{m}^{-1}$ antenna phasing did not have a significant effect in this experiment.

This discrepancy between theory and experiment, which was repeatable during this run day, is currently not understood. The antenna performance and reliability have recently been significantly improved, so this will be reinvestigated in the next NSTX campaign.

III. DATA ANALYSIS

Many different codes were used to analyze the experimental data. As a primary method, the TRANSP transport analysis code was used to calculate fast ion energy and particle density profiles. This information was used to estimate an effective Maxwellian temperature for the fast ion population. Figure 10 demonstrates that a single effective Maxwellian, matching fast ion particle and energy density exactly, fits the TRANSP $f(E)$ remarkably well. These profiles, along with EFIT (Refs. 10–12) and Thomson scattering[13] electron density and temperature data, were fed into HPRT, a 2D ray-tracing code which uses the full hot plasma dielectric with complex $\mathbf{k}$ to compute power deposition profiles along the hot electron/cold ion ray path.[8] This code is described more completely in Ref. 14. Unfortunately, no CHERS data were available for this series of shots, so for the thermal ion temperature an approximation of $T_i=2T_e$ was made, based on a general estimate from the X-Ray Crystal Spectrometer[15] in beam-heated NSTX plasmas. This should pose little difficulty since thermal ion absorption was calculated to be insignificant in this series of shots, and no experimental evidence of thermal ion absorption has yet been found.

CQL3D,[16] a quasilinear Fokker–Planck code, was also particularly important in examining the effects of HHFW on the fast ion distribution function. Its output was interfaced with a TRANSP-based NPA simulator to compare with measured NPA spectra, and both codes were used to compare measured with simulated neutron rates. This simulator is also described more completely in Ref. 14.

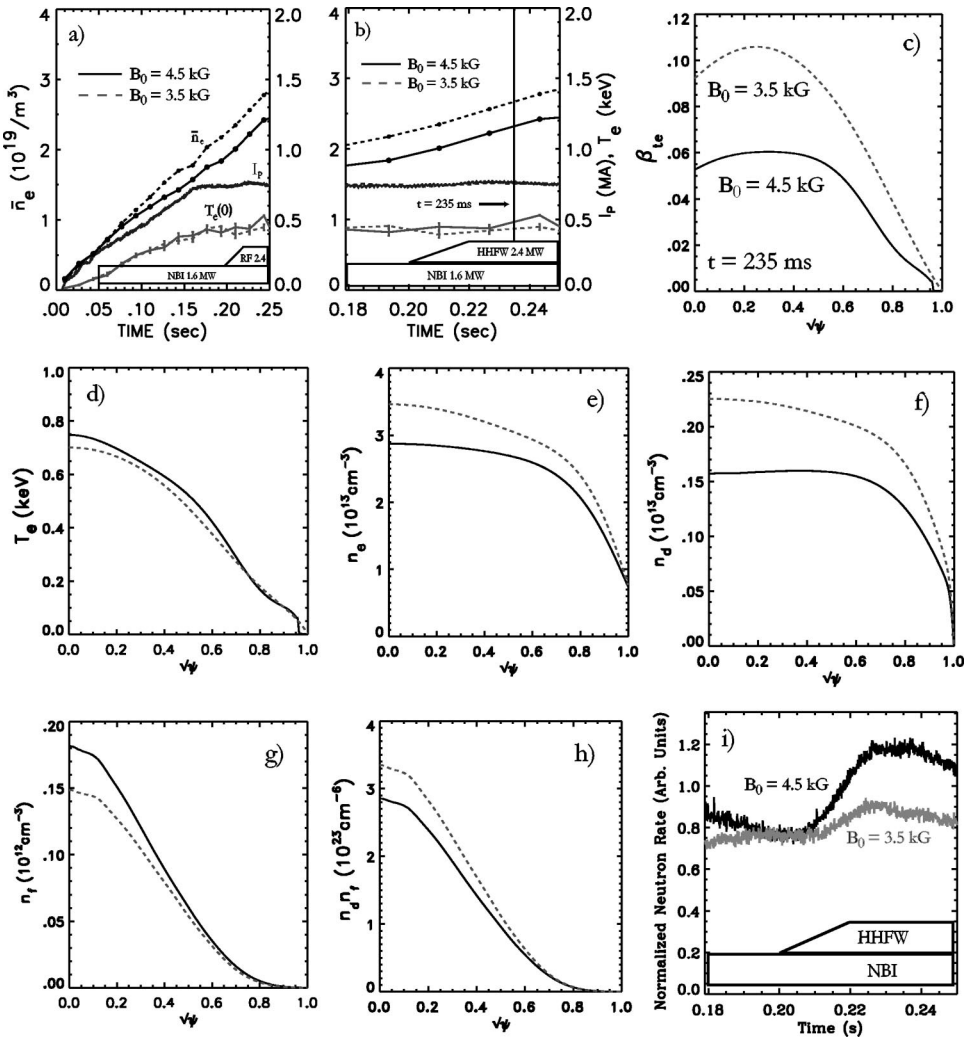

FIG. 7. (a) Line-averaged electron density, temperature, plasma current, NBI, and rf power histories for NSTX shots 108251 ($B_0 = 4.5$ kG, lower β) and 108252 ($B_0 = 3.5$ kG, higher β). (b) Expansion of (a) from 180 ms to 250 ms. (c) Outer midplane β_{te} profiles vs $\sqrt{\psi}$, a radial coordinate, at $t = 235$ ms. This difference between these two shots is the most prominent. (d) Electron temperature and (e) density profiles. (f) Thermal deuterium densities n_d, derived from assuming quasineutrality, 5% hydrogen, a flat carbon impurity profile from measured Z_{eff}, and using the TRANSP code to determine fast deuterium density. (g) Fast deuterium density n_f profiles. (h) $n_d \times n_f$ profiles. (i) Neutron rates from Fig. 6(a) normalized to $n_d(0,t) \times n_f(0,t)$. This result indicates that the measured neutron rate difference might have been larger if the densities were equal.

A. rf vs no rf comparisons

Without taking into account the rf input, TRANSP was used to calculate the neutron rates for similar rf and no-rf shots. As shown in Fig. 11, the measured rate matched the prediction well in the no-rf case before a large reconnection event at $t = 226$ ms, and for the rf shot grew to nearly double the predicted rate. It then decayed to approximately the computed rate after rf turnoff.

CQL3D was used to simulate the neutron rate evolution in shots with and without rf, as shown in Fig. 12(a). Unfortunately, CQL3D cannot currently input time-dependent magnetic or kinetic equilibria, so these effects, particularly evident in the measured trace of no-rf shot 108269, are unable to be captured. Also, the uncertainty in the voltage calibration factor in the ZnS neutron detectors is at least $\pm 10\%$. Time slice $t = 235$ ms was chosen for the equilibria used in the simulation as this time is well into rf injection and the plasma current flat top, though before a MHD event at $t = 240$ ms, thereby making it a favorable time to compare the NPA simulator with its 10 ms averaged measurement. If time $t = 180$ ms is chosen, the simulated absolute no-rf neutron rate matches the measurement well at the beginning of the time window displayed in Fig. 12(a) rather than the end, and general trends remain unchanged. For completeness, composite CQL3D neutron rates linearly time-weighted using the two calculated solutions from equilibria at $t = 180$ and 235 ms are shown in Fig. 12(b). While a better match is found, it should be noted that the effect of significant changes to equilibrium parameters prior to $t = 180$ ms are not captured here. TRANSP simulations for the same shots are shown in Fig. 12(c). TRANSP does use time-dependent profiles, however, it currently has no model to take into account the effect of HHFW absorption on the fast ion distribution function. It is noteworthy that TRANSP therefore predicts the no-rf rate to actually exceed the rf rate for these shots.

The neutron rate ratio between rf and no-rf rates for both measurement and simulation are shown in Fig. 13(a). As the relative calibration factor between shots in this series is essentially 1.0, this plot eliminates the absolute calibration factor uncertainty, however, the lack of time dependence remains an issue. Still, the trend of a higher ratio after rf turn-on is maintained in both. Figure 13(b) shows the same ratio, using half the experimentally injected rf power in the simulation. Better agreement is found, indicating that edge absorption of HHFW, which has recently been observed on NSTX in Ref. 17, may be significant.

Results for rf vs no-rf shots in comparison with measurements using CQL3D's distribution function in the NPA simu-

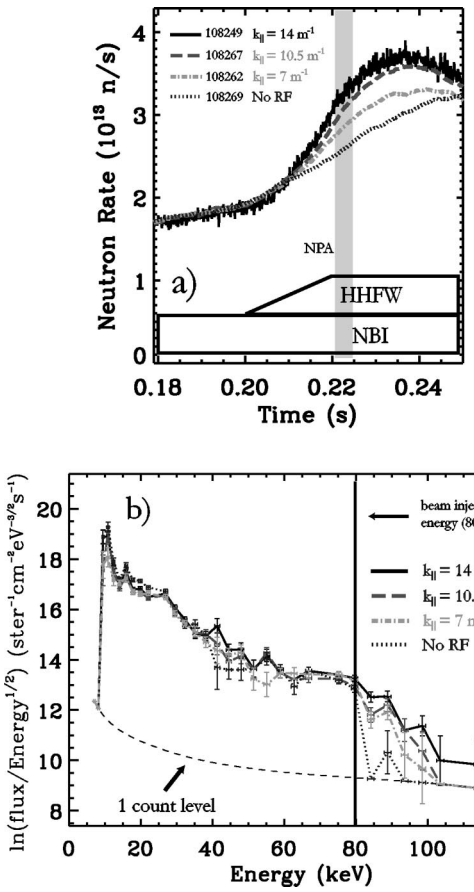

FIG. 8. (a) Neutron rates for NSTX shots 108249 (Launched toroidal mode number $|N_\phi| = 24.0$, which roughly corresponds to launched $k_\parallel = 14\ m^{-1}$), 108267 ($|N_\phi| = 18.0$, launched $k_\parallel \approx 10.5\ m^{-1}$), 108262 ($|N_\phi| = 12.0$, launched $k_\parallel \approx 7\ m^{-1}$), and 108269 (no-rf). (b) NPA signals at $R_{tan} = 70$ cm for $k_\parallel$ scan, averaged over time window displayed in (a). Observed trends are opposite to theory prediction of less ion absorption at higher $k_\parallel$.

lator are shown in Figs. 14(a) and 14(b). These shots have a NPA tangency radius of $R_{tan} = 70$ cm. Simulator vs measurement results for one shot at $R_{tan} = 90$ cm with and without rf input to the simulator are shown in Figs. 15(a) and 15(b). Unfortunately, CQL3D's beam package, FREYA, does not cur-

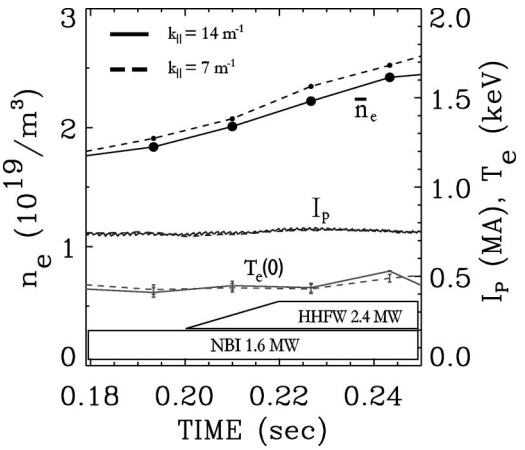

FIG. 9. Line-averaged density, temperature, plasma current, NBI, and rf power histories for NSTX shots 108251 ($k_\parallel \approx 14\ m^{-1}$) and 108260 ($k_\parallel \approx 7\ m^{-1}$). They are very similar.

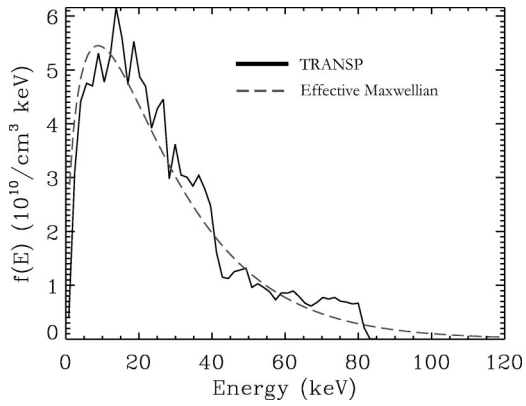

FIG. 10. TRANSP $f(E)$ for NSTX shot 108251, $t = 235$ ms at $\sqrt{\psi} = 3\%$ vs an effective Maxwellian matching its total energy and particle density exactly. The agreement is similar out to $\sqrt{\psi} \sim 70\%$, beyond which the Monte Carlo statistics in TRANSP become particularly noisy.

rently handle finite larmor orbit effects, which are quite substantial in a ST. (NSTX larmor radii can be ~15 cm or more for fast ions.) This leads to an unphysical localization of its fast ion distribution function in pitch angle space near the beam injection pitch angle. To suppress this localization the

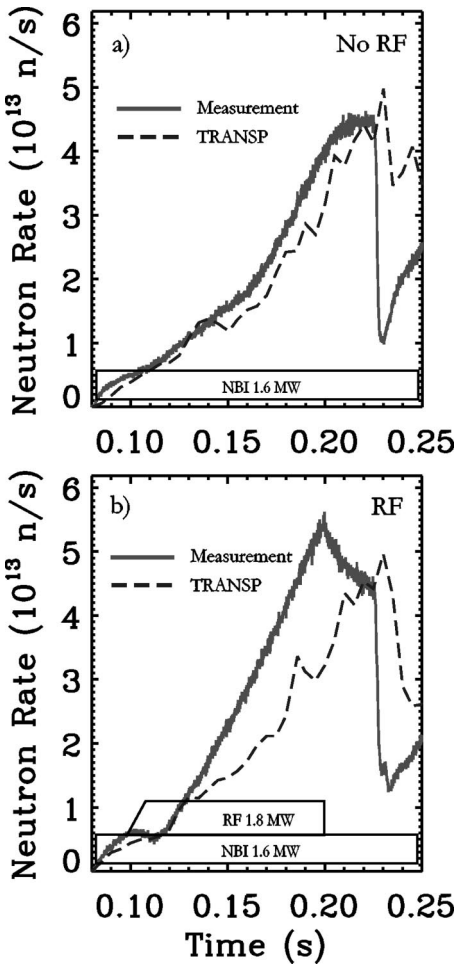

FIG. 11. (a) Neutron rate for no-rf shot 105906 vs TRANSP prediction. (b) Same for rf shot 105908 vs TRANSP prediction. Measured neutron rate for rf shot significantly exceeds TRANSP prediction without rf input. After rf turns off, rate decays close to measured and predicted no-rf value. TRANSP currently has no model to determine effect of HHFW on its fast ion distribution function, so this is a consistent result.

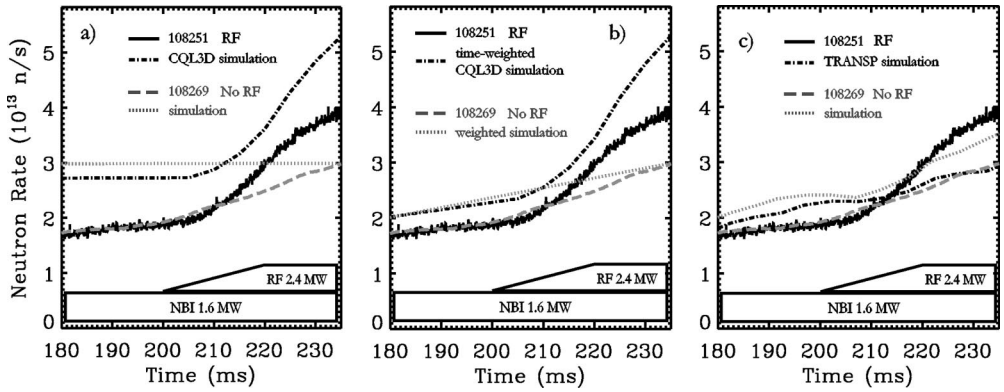

FIG. 12. (a) Measured vs CQL3D simulated neutron rates for otherwise similar NSTX shots 108251 (rf) and 108269 (no-rf). The uncertainty in the voltage calibration factor in the ZnS neutron detectors is at least ±10%, and time-dependent kinetic and magnetic profiles are not currently possible in the model, so profiles at $t=235$ ms are used. (b) Composite time-weighted CQL3D neutron rates using independent solutions, one from an equilibrium at $t=180$ ms, the other from $t=235$ ms. (c) TRANSP simulations for the same shots. TRANSP does use time-dependent profiles, however, it currently has no model to take into account HHFW power absorption on fast ions. Note that TRANSP therefore predicts the no-rf rate to actually exceed the rf rate for these shots.

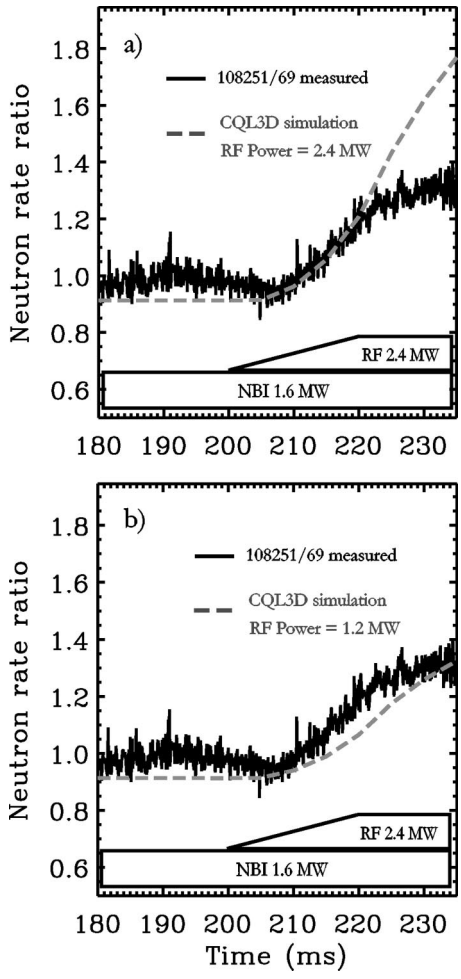

FIG. 13. (a) Neutron rate ratio between NSTX shots 108251 (rf) and 108269 (no-rf) for both measurement and simulation using magnetic and kinetic profiles at $t=235$ ms. This eliminates the absolute calibration factor uncertainty, however, the lack of time dependence is still an issue. The trend of a higher ratio after rf turn-on is maintained in both. (b) The same, using half the rf power injected. Better agreement is found, indicating edge absorption may be significant.

distribution function at each energy above 20 keV from $\chi = v_{\parallel}/v = 0$ to 1 has been averaged. To demonstrate the difference, Figs. 14(a) and 15(a) are not averaged, and Figs. 14(b) and 15(b) are. It is subjective whether one considers the averaged simulation closer to measurement for shot 108249 in Fig. 14(a) vs. Fig. 14(b), which is close to the beam's tangency radius of 69.4 cm, where the average

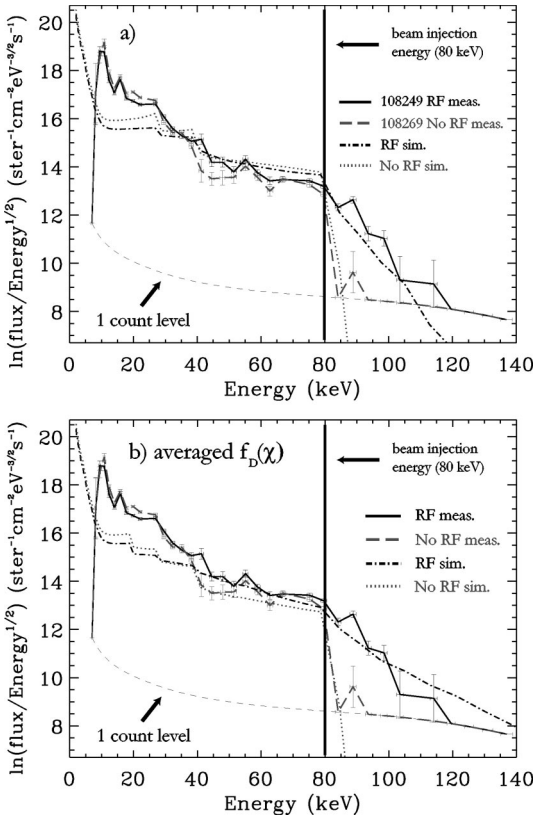

FIG. 14. (a) NPA measurements for shots 108249 (rf) and 108269 (no-rf), averaged from 220 to 230 ms, compared with simulator results for these shots at 225 ms. The NPA tangency radius for these shots is 70 cm. (b) Same, using a fast ion distribution function smeared in pitch angle space to account for lack of FLR effects in CQL3D's beam model.

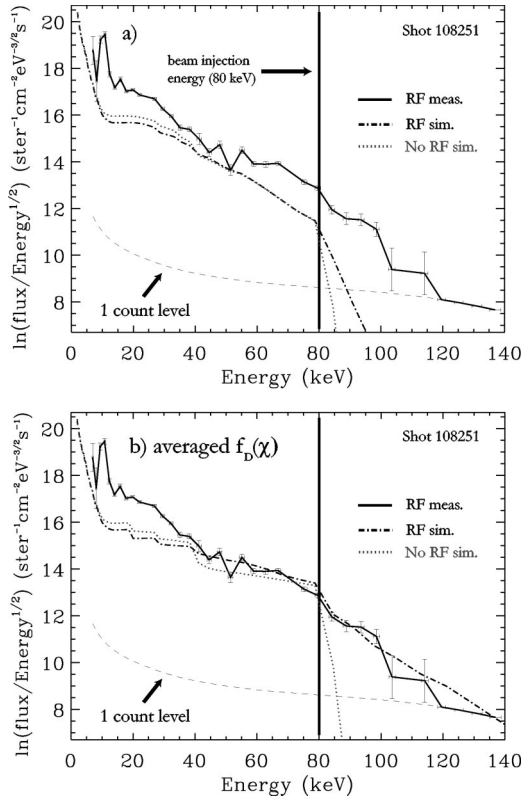

FIG. 15. (a) NPA measurements for shot 108251, averaged from 230 to 240 ms, compared with simulator results with and without rf input at 235 ms. The NPA tangency radius for this shot is 90 cm. (b) Same, using a fast ion distribution function smeared in pitch angle space to account for lack of FLR effects in CQL3D's beam model. Simulator plots from here on will use a similarly treated distribution function.

should be less important. However, for a tangency radius of 90 cm where the average should be more important, the averaged fast ion tail in Fig. 15(b) is clearly a closer fit than Fig. 15(a). From here on, the averaged distribution function is used when presenting simulation results.

Figure 16 demonstrates the effect of variation in the total injected rf power on the output from the NPA simulator. The hatched region displays the range of simulator results using half to the full experimentally injected rf power. This range approaches the error bars in the tail measurement and, in agreement with the neutron rate comparisons shown in Fig. 13, also suggests that a significant portion of injected rf power may be lost before reaching the bulk plasma.

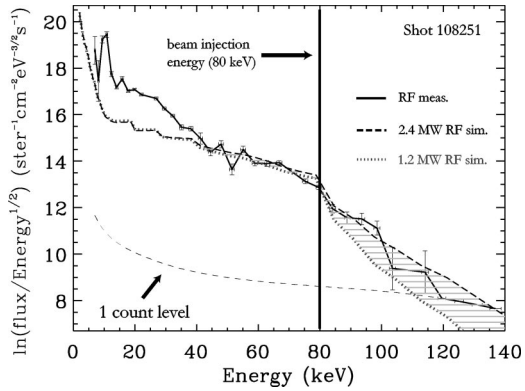

FIG. 16. NPA measurements for shot 108251, averaged from 230 to 240 ms, compared with simulator results with half-to-full injected rf power at 235 ms. This range approaches the error bars in the tail measurement, and indicates that a significant portion of injected rf power may be lost before reaching the bulk plasma.

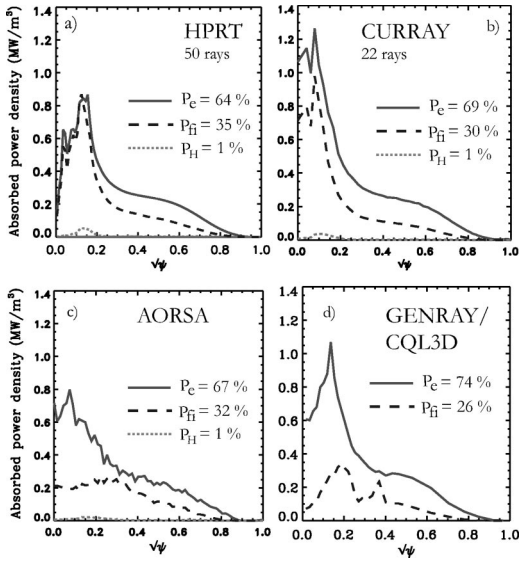

FIG. 17. Power deposition profiles for NSTX shot 108251, $t=235$ ms, $N_\phi=24$ from (a) HPRT, 50 rays, (b) CURRAY, 22 rays, (c) AORSA, and (d) GENRAY/CQL3D. Here P_e is the absorbed power fraction on electrons, P_{fi} is absorbed power on fast deuterium, and P_H is thermal hydrogen. Thermal carbon absorption was calculated to be insignificant. Analytic approximations for the measured radial kinetic profiles were used in this comparison. Good agreement is found in fractional absorption and deposition profiles between codes for rf+NBI shots.

It is worth noting that after taking geometric differences into account these plots are not otherwise corrected or normalized. Considering the neutral profiles calculated in TRANSP have a high degree of uncertainty—they are completely unmeasured and a 1D model is used for the thermal and cold neutrals—the matches are quite satisfactory. Given the quantitative matching of the NPA signals for energies greater than 80 keV, we conclude that the observed fast ion tail induced by the high harmonic fast wave likely follows from currently understood wave theory. The larger discrepancy below ~30 keV is likely due to greater uncertainty in the wall neutral model.

B. Code comparison

As shown in Fig. 17, fast ion absorption was calculated to be competitive with electron absorption in sustained neutral beam shots, often amounting to ~30%–50% of the total rf power. Figures 17(a)–17(d) show that results from HPRT matched those of CURRAY,[18] an independently developed ray-tracing code, AORSA,[19] an all orders full wave code, and CQL3D reasonably well for rf+NBI equilibria. CQL3D uses a model of the fast ion distribution function rather than an effective Maxwellian, so its input information is not identical to the other codes. Also, it currently cannot calculate absorption on more than 3 consecutive harmonics at a time, so the total fast ion absorption is likely larger. In this case 9 through 11 were chosen as the field on-axis is near the ninth harmonic, the ray paths are clustered on the outboard side of the

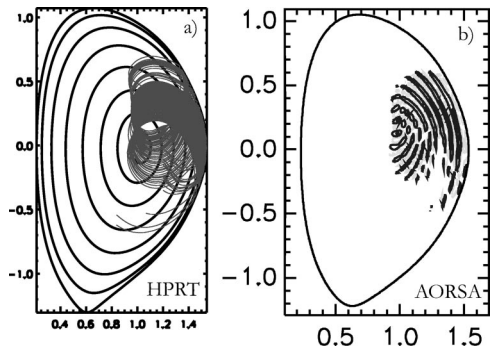

FIG. 18. (a) 50 HPRT ray paths, with initial positions distributed evenly over poloidal range of antenna, for NSTX shot 108251, $t=235$ ms, $\beta=5.2\%$, $N_\phi=24$. Each ray stops when 99% of its power is absorbed. (b) AORSA wave fronts for the same shot.

plasma, and the fast ion density is centrally localized. It should be noted that AORSA predicts absorption on the twelfth harmonic to be significant as well, however. Diffraction and interference effects, only included in a full wave code, may account for the difference between the AORSA and the ray-tracing code predictions near the core of the plasma.

A comparison of typical ray paths in HPRT vs wavefront propagation calculated by AORSA is shown in Fig. 18. Both codes launch waves from identical antenna geometry on the outboard side of the plasma. The flow of these paths are remarkably similar considering the quite different methods of calculation. This supports the use of ray-tracing for these experiments, and also helps demonstrate the importance of including 2D effects in absorption calculations for ST equilibria.

C. Magnetic field scan

Figure 19 shows the HPRT-calculated deposition profiles for the experimental magnetic field scan. Lower on-axis absorption is calculated for lower B, or higher β, in agreement with the neutron rate and NPA signals in Fig. 6, as the greater off-axis electron absorption in higher β shots prevents as much rf power from reaching the bulk of the fast ion population near the magnetic axis. TRANSP calculates fast ion density to be centrally peaked.

Providing further support for this conclusion, NPA spectra from CQL3D/TRANSP and measurements are shown in Fig. 20. Measured and CQL3D simulated neutron rate traces are shown in Fig. 21(a), and to eliminate absolute calibration factor uncertainty, neutron rate ratios are shown in Fig. 21(b). These simulations predict the rf-enhanced fast ion tail and neutron rate to be suppressed at higher β, in good agreement with measurement.

An increased fast ion loss fraction at lower B may also contribute to suppression of the observed tail, so loss codes EIGOL[20] which follows the full fast ion orbit, and CONBEAM,[21] which follows the guiding center of the orbits and accounts for finite larmor radius effects, were used to determine the significance of this factor. For 120 keV ions, EIGOL calculates a loss fraction of 17% for a $B_0=4.5$ kG equilibrium—NSTX shot 108250, $t=235$ ms, and 23% for $B_0=3.5$ kG—shot 108252, $t=235$ ms. CONBEAM calculates

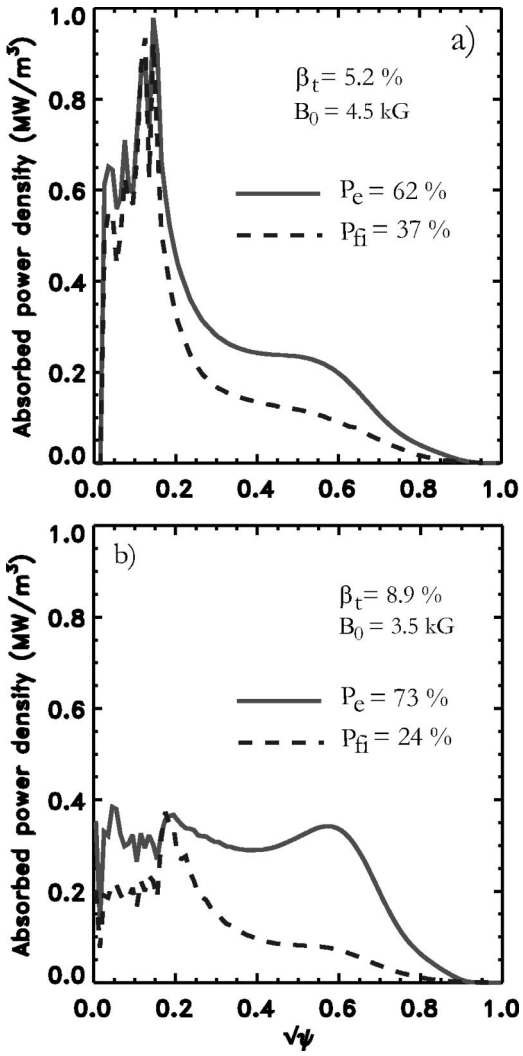

FIG. 19. (a) HPRT power deposition profiles for NSTX shot 108250, $t=230$ ms, $B_0=4.5$ kG, $\beta_t=5.2\%$. (b) Shot 108252, $t=230$ ms, $B_0=3.5$ kG, $\beta_t=8.9\%$. Lower on-axis absorption is calculated for lower B, higher β, in agreement with neutron rate and NPA signals.

a loss fraction of 21% for $B_0=4.5$ kG, and 25% for $B_0=3.5$ kG. According to the NPA data, the tail is suppressed by at least a factor of 8 between high and low field, so the tail reduction is much more likely due to an rf effect.

D. $k_\parallel$ scan

Calculated absorption profiles from HPRT for otherwise well matched shots with toroidal mode numbers $N_\phi=24.0$ and 12.0 are shown in Figs. 22(a) and 22(b). $N_\phi=24.0$ roughly corresponds to launched $|k_\parallel|\approx 14\,\mathrm{m}^{-1}$, while $N_\phi=12.0$ roughly corresponds to $|k_\parallel|\approx 7\,\mathrm{m}^{-1}$. Significantly more fast ion absorption is predicted at lower $k_\parallel$.

NPA spectra from CQL3D/TRANSP and measurements are shown in Fig. 23. Measured and CQL3D simulated neutron rate traces are shown in Fig. 24(a), and to eliminate absolute calibration factor uncertainty, neutron rate ratios are shown in Fig. 24(b). For both the NPA and neutron rate comparisons, a significantly larger rf-induced tail and neutron rate are predicted at lower $k_\parallel$, which is the opposite of what is

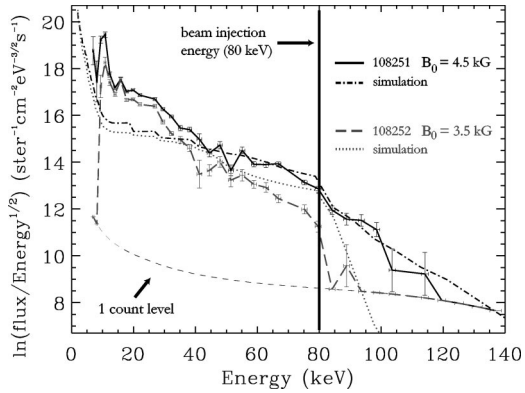

FIG. 20. NPA measured spectra vs CQL3D/TRANSP simulation for NSTX shots 108251-$B_0=4.5$ kG, $\beta_t=5.2\%$, and 108252-$B_0=3.5$ kG, $\beta_t=8.9\%$. Measured signals are averaged from 230 to 240 ms, and the simulation output is at 235 ms. In agreement with measurement, the simulator finds a reduced tail at larger β_t.

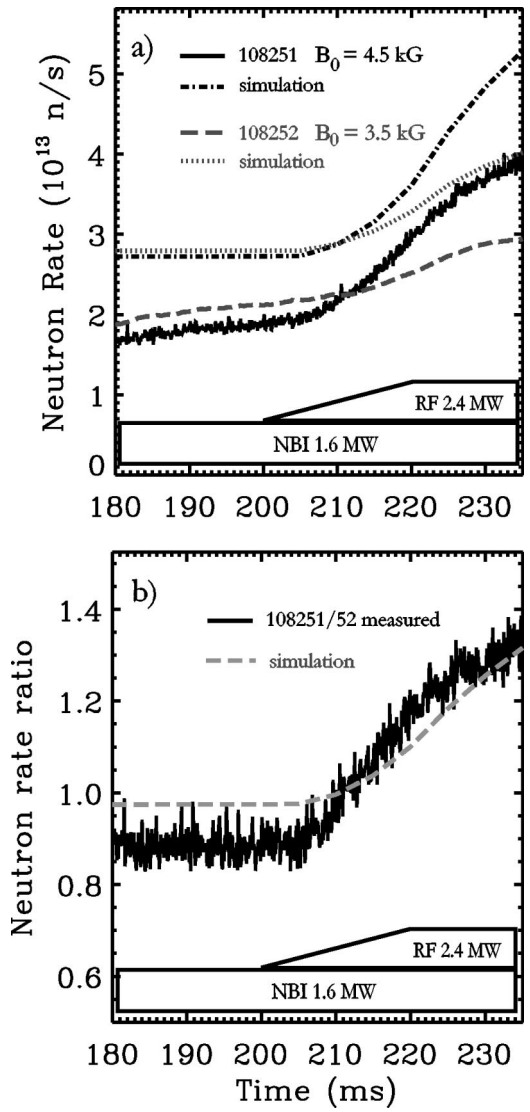

FIG. 21. (a) Measured vs CQL3D simulated neutron rates for NSTX shots 108251-$B_0=4.5$ kG, $\beta_t\approx5.2\%$, and 108252-$B_0=3.5$ kG, $\beta_t\approx8.9\%$. Magnetic equilibria and kinetic profiles at $t=235$ ms are used. In agreement with measurement, the simulator finds a lower neutron rate at larger β_t. (b) Neutron rate ratio between high and low B_0 rates for both measurement and simulation, eliminating calibration factor uncertainty. Very similar ratio traces are found.

measured. The effect of the observed edge ion absorption[17] on the wave spectrum that reaches the bulk plasma has yet to be determined.

For equilibria without fast ions, low $N_\phi\approx6$, and high thermal $T_i(0)\approx2$ keV, less agreement between wave absorption codes has been found, often differing in bulk deuterium absorption by a factor of ~2, with HPRT consistently calculating less than CURRAY or AORSA. For example, for a particular shot 108901 at $t=300$ ms without netural beams, HPRT calculates 11% bulk deuterium absorption and CURRAY calculates 19%. This is surprising considering the level of agreement for the fast ion shots which actually had $T_i(0)\approx1.5$ keV. CURRAY and HPRT have been found to agree in ray path and deposition profile quite well for rf+NBI and equilibria dominated by electron absorption. AORSA also calculates $\sim19\%$ bulk ion absorption in this case, however, greater agreement is expected between the ray-tracing codes than between either one and a full wave code. A possible explanation is that HPRT is using the complex $\mathbf{k}$ in its dielectric tensor, whereas CURRAY does not, and the impact only arises in this particular parameter regime. As derived in Ref. 14, HPRT's equation for absorbed power density

$$\frac{\partial W_{\mathrm{ps}}}{\partial t}=\mathbf{E}_1^*\cdot\mathbf{j}_s-\nabla\cdot\mathbf{T}_s \tag{1}$$

thus includes the latter kinetic flux term:

$$\nabla\cdot\mathbf{T}_s=\frac{\omega}{8\pi}\mathbf{E}_1^*\cdot\left(\mathbf{k}_i\cdot\frac{\partial}{\partial\mathbf{k}}\bar{\bar{\epsilon}}_{Hs}\cdot\mathbf{E}_1\right)e^{2\phi_i}, \tag{2}$$

while CURRAY, because it keeps k real in the evaluation of its dielectric tensor, sets $\partial W_{\mathrm{ps}}/\partial t=\mathbf{E}_1^*\cdot\mathbf{j}_s$. It should be noted that a rigorous derivation from the energy moment of the Vlasov equation to this form of the kinetic flux term with complex $\mathbf{k}$ has yet to be performed. Noting that there is currently discrepancy between theory and experiment in the $k_\parallel$ scan (there has yet to be any experimental evidence of significant bulk ion absorption at all in NSTX), and there is a discrepancy between ray-tracing codes at lower $k_\parallel$, a breakdown of the theory at lower $k_\parallel$ should not be ruled out. The ion damping model may need to be carefully re-examined for its dependence on $k_\parallel$ in general.

IV. CONCLUSIONS AND FUTURE WORK

Analysis of recent NSTX shots has revealed that under some conditions when neutral beam and rf power are injected into the plasma simultaneously, a fast ion population above the beam injection energy is sustained by the wave. A significant neutron rate enhancement is also observed. A TRANSP-based NPA simulator coupled to the quasilinear Fokker–Planck code CQL3D indicates that this rf-induced tail likely follows from currently understood wave theory.

Also in agreement with modeling, these experiments find the rf-induced fast ion tail strength and neutron rate at lower

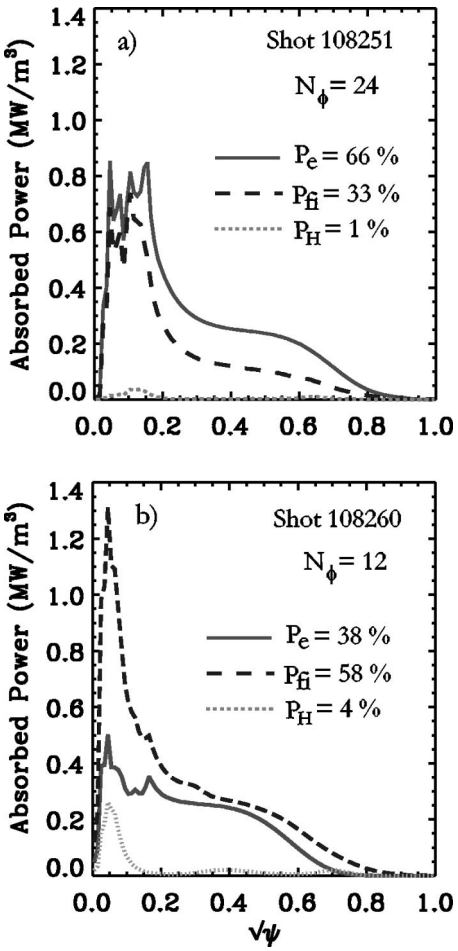

FIG. 22. (a) HPRT power deposition profiles for NSTX shot 108251, $t = 235$ ms, $N_\phi = 24.0$, $|k_\parallel| \approx 14\ \mathrm{m}^{-1}$. (b) Shot 108260, $N_\phi = 12.0$. Significantly more fast ion absorption is predicted at lower $k_\parallel$.

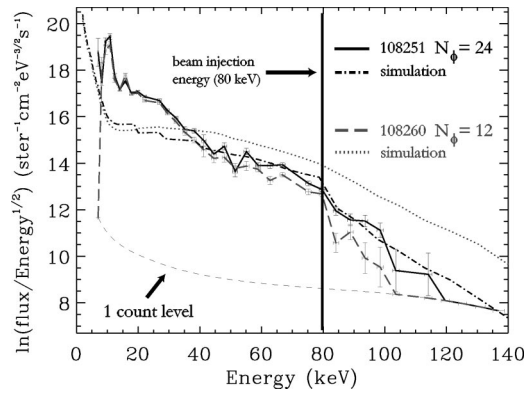

FIG. 23. (a) Measured and simulated NPA spectra for NSTX shot 108251, $N_\phi = 24.0$, $|k_\parallel| \approx 14\ \mathrm{m}^{-1}$ vs 108260 with $N_\phi = 12.0$. Measured signals are averaged from 230 to 240 ms, and the simulation output is at 235 ms. A significantly larger rf-induced tail is predicted at lower $k_\parallel$, in contrast to measurement.

B-fields to be less enhanced, likely due to a larger β profile, which promotes greater off-axis absorption where the fast ion population is small. Ion loss codes EIGOL and CONBEAM find the increased loss fraction with decreased magnetic field insufficient to account for the changes in tail strength, providing further evidence that this is an rf interaction effect.

Though greater ion absorption, a much larger fast ion tail, and a higher neutron rate are predicted with lower $k_\parallel$, surprisingly little variation in the tail was observed, and the neutron rate enhancement was greater with higher, not lower $k_\parallel$. This discrepancy will be re-examined with the recently upgraded rf antenna system in the upcoming NSTX campaign under improved plasma conditions.

Comparison between ray-tracing codes HPRT and CURRAY, full-wave code AORSA, and CQL3D have found good agreement in deposition profile and fractional absorption for rf+NBI shots. Ray paths and wave fronts match remarkably well between the ray-tracing codes and AORSA. Less agreement is found between HPRT and CURRAY in lower $k_\parallel$, no-NBI equilibria with high thermal ion temperatures.

Implications for heating a reactor ST are favorable. On the one hand, electron absorption is preferred, as current drive is more efficient for electrons than ions, so any ion absorption is considered parasitic. On the other, the β scan results are encouraging. A reactor ST will have a much larger β profile than a typical NSTX shot, so it may very well have

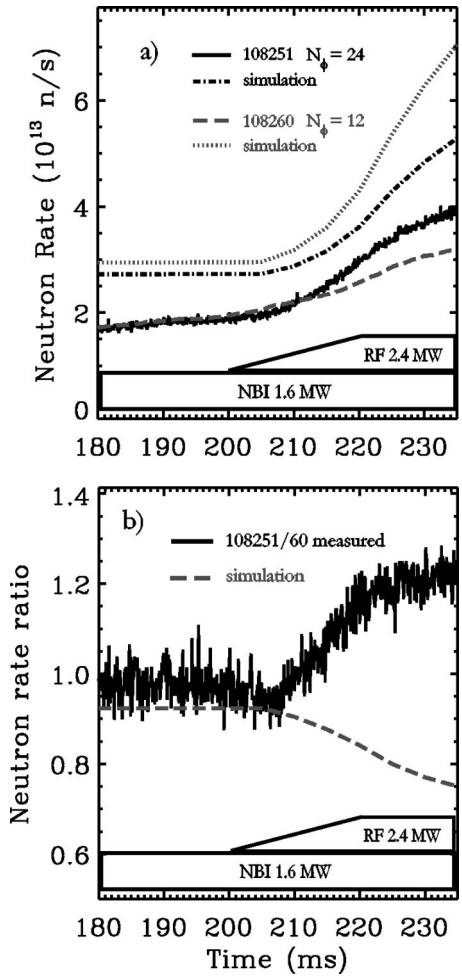

FIG. 24. (a) Measured vs CQL3D simulated neutron rates for NSTX shot 108251, $N_\phi = 24.0$, $|k_\parallel| \approx 14\ \mathrm{m}^{-1}$ vs 108260 with $N_\phi = 12.0$. Magnetic equilibria and kinetic profiles at $t = 235$ ms are used in the simulation. (b) Neutron rate ratio between high and low N_ϕ rates for both measurement and simulation, eliminating calibration factor uncertainty. A significantly larger neutron rate is predicted at lower $k_\parallel$, in sharp contrast to measurement.

a significantly lower fast ion (in this case alpha-particle) absorption fraction than demonstrated here. As for the $k_{\|}$ scan results, there was initially concern that at lower $k_{\|}$, where NSTX's antenna has directional variability for current drive studies, strong ion absorption could be a serious issue, however this does not currently appear to be the case. Still, further investigation in hotter, more stable plasmas with larger plasma currents is certainly warranted.

There are several possible avenues of future work. CQL3D's applicability to ST plasmas will improve when it can calculate absorption on more than 3 consecutive harmonics, include FLR effects in its beam package, read asymmetric equilibria, and utilize time-dependent magnetic equilibria and kinetic profiles. TRANSP includes a great deal of physics that CQL3D does not, such as FLR effects, asymmetric equilibria, time-dependent profiles, and neutral information. However, it currently has no package to deal with high harmonic fast wave injection's effect on the fast ion distribution function. Perhaps CQL3D should be incorporated into TRANSP. HPRT may be more accurate in its absorption calculation if its dielectric elements were modified to read in shifted Maxwellians, as well as parallel and perpendicular temperatures. As for experimental work, the $k_{\|}$ scan should be revisited with the improved antenna system, and a greater β range with rf and beams should be explored, perhaps in an H-mode vs L-mode comparison. Also, the neutral particle analyzer for shots examined in this paper could only be horizontally scanned on the inboard side of the plasma, so interpretation of its signal was obscured by the contributions from the plasma core, as well as the inboard and outboard side. Signals from an outboard scan of the plasma, now possible due to upgrades of the NPA hardware, should yield more easily interpreted results.

One interesting consequence of alpha particle absorption of rf power in a reactor is the so-called ''alpha channeling'' effect, in which alpha particles are ejected from the tokamak as they give up energy to rf waves.[22,23] The effect can happen in a ST as well, so long as waves traveling in one toroidal direction only are employed. The ratio of the change in canonical angular momentum (which can be related to the radial distance traversed to energy extracted) scales with the toroidal mode number N_{ϕ}.[24,25] For NSTX, modes such that $N_{\phi}=4$ would move alpha particles fully to the periphery while extracting essentially all their energy. This is lower than the current typical experimental values of 12–24 on NSTX, though accessible with current antenna technology, making the alpha channeling effect an interesting possibility in ST reactors.

ACKNOWLEDGMENT

This research is supported by the U.S. Department of Energy under Contract No. DE-AC02-CHO3073.

[1] Y.-K. M. Peng and D. J. Strickler, Nucl. Fusion **26**, 769 (1986).
[2] M. Ono, Phys. Plasmas **2**, 4075 (1995).
[3] M. Ono, S. M. Kaye, Y.-K. M. Peng *et al.*, Nucl. Fusion **40**, 557 (2000).
[4] S. S. Medley and A. L. Roquemore, Rev. Sci. Instrum. **69**, 2651 (1998).
[5] J. R. Wilson, R. E. Bell, S. Bernabei *et al.*, Phys. Plasmas **10**, 1733 (2003).
[6] R. J. Hawryluk, in *Physics of Plasmas Close to Thermonuclear Conditions*, in *Proceedings of the International School of Plasma Physics*, edited by B. Coppi, G. Leotta, D. Pfirsch, R. Pozzoli, and E. Sindoni (Pergamon, Varenna, Italy, 1981), Vol. 1, p. 19.
[7] J. P. H. E. Ongena, M. Evrard, and D. McCune, Fusion Technol. **33**, 181 (1998).
[8] J. Menard, R. Majeski, R. Kaita, M. Ono, and T. Munsat, Phys. Plasmas **6**, 2002 (1999).
[9] C. N. Lashmore-Davies, V. Fuchs, and R. A. Cairns, Phys. Plasmas **5**, 2284 (1998).
[10] L. Lao, H. St. John, R. Stambaugh, A. Kellman, and W. Pfeiffer, Nucl. Fusion **25**, 1611 (1985).
[11] S. A. Sabbagh, S. M. Kaye, J. Menard *et al.*, Nucl. Fusion **41**, 1601 (2001).
[12] S. A. Sabbagh, R. E. Bell, M. G. Bell *et al.*, Phys. Plasmas **9**, 2085 (2002).
[13] B. P. LeBlanc, R. E. Bell, D. W. Johnson, D. E. Hoffman, D. C. Long, and R. W. Palladino, Rev. Sci. Instrum. **74**, 1 (2003).
[14] A. L. Rosenberg, Ph.D. thesis, Princeton University, 2003.
[15] M. Bitter, K. Hill, L. Roquemore, P. Beiersdorfer, D. Thorn, and M. F. Gu, Rev. Sci. Instrum. **74**, 1977 (2003).
[16] R. W. Harvey and M. G. McCoy, in *Proceedings of IAEA Technical Committee Meeting on Advances in Simulation and Modeling of Thermonuclear Plasmas* (IAEA, Montreal, 1992), available through USDOC, NTIS No. DE9300962.
[17] T. M. Biewer, R. E. Bell, D. S. Darrow, and J. R. Wilson, in *Radio Frequency Power in Plasmas: 15th Topical Conference*, AIP Conf. Proc. 694 (American Institute of Physics, New York, 2003).
[18] T. K. Mau, C. C. Petty, M. Porkolab, and W. W. Heidbrink, in *Radio Frequency Power in Plasmas: 13th Topical Conference*, AIP Conf. Proc. 485 (American Institute of Physics, New York, 1999), p. 148.
[19] E. F. Jaeger, L. A. Berry, E. D'Azevedo, D. B. Batchelor, and M. D. Carter, in *Radio Frequency Power in Plasmas: 14th Topical Conference*, AIP Conf. Proc. 595 (American Institute of Physics, New York, 2001), p. 369.
[20] D. S. Darrow, R. Akers, D. Mikkelsen, S. Kaye, and F. Paoletti, in *Proceedings of the 6th IAEA Technical Committee Meeting on Energetic Particles in Magnetic Confinement Systems* (Japan Atomic Energy Research Institute, Ibaraki-ken, Japan, 2000), p. 109.
[21] J. Egedal, M. H. Redi, D. S. Darrow, and S. M. Kaye, Phys. Plasmas **10**, 2372 (2003).
[22] N. J. Fisch and J. M. Rax, Phys. Rev. Lett. **69**, 612 (1992).
[23] N. J. Fisch and M. C. Herrmann, Plasma Phys. Controlled Fusion **41**, A221 (1999).
[24] N. J. Fisch and M. C. Herrmann, Nucl. Fusion **35**, 1753 (1995).
[25] M. C. Herrmann, Ph.D. thesis, Princeton University, 1998, p. 91.